

Fluctuation-dissipation relations in the imbalanced Wilson-Cowan modelManoj Kumar Nandi ¹, Antonio de Candia ^{2,3}, Alessandro Sarracino ^{1,4},
Hans J. Herrmann ^{5,6} and Lucilla de Arcangelis ^{7,*}¹*Department of Engineering, University of Campania “Luigi Vanvitelli” 81031 Aversa (Caserta), Italy*²*Department of Physics “E. Pancini”, University of Naples Federico II, 80126 Naples, Italy*³*INFN, Section of Naples, Gruppo collegato di Salerno, 84084 Fisciano, Italy*⁴*Institute for Complex Systems–CNR, Piazzale Aldo Moro 2, 00185 Rome, Italy*⁵*PMMH, ESPCI, 7 quai St. Bernard, Paris 75005, France*⁶*Department of Physics, Federal University of Ceará, Fortaleza, Ceará 60451-970, Brazil*⁷*Department of Mathematics & Physics, University of Campania “Luigi Vanvitelli” Viale Lincoln, 5, 81100 Caserta, Italy*

(Received 29 November 2022; revised 17 April 2023; accepted 15 May 2023; published 15 June 2023)

The relation between spontaneous and stimulated brain activity is a fundamental question in neuroscience which has received wide attention in experimental studies. Recently, it has been suggested that the evoked response to external stimuli can be predicted from temporal correlations of spontaneous activity. Previous theoretical results, confirmed by the comparison with magnetoencephalography data for human brains, were obtained for the Wilson-Cowan model in the condition of balance of excitation and inhibition, a signature of a healthy brain. Here we extend previous studies to imbalanced conditions by examining a region of parameter space around the balanced fixed point. Analytical results are compared to numerical simulations of Wilson-Cowan networks. We evidence that in imbalanced conditions the functional form of the time correlation and response functions can show several behaviors, exhibiting also an oscillating regime caused by the emergence of complex eigenvalues. The analytical predictions are fully in agreement with numerical simulations, validating the role of cross-correlations in the response function. Furthermore, we identify the leading role of inhibitory neurons in controlling the overall activity of the system, tuning the level of excitability and imbalance.

DOI: [10.1103/PhysRevE.107.064307](https://doi.org/10.1103/PhysRevE.107.064307)**I. INTRODUCTION**

The brain is a complex system whose properties emerge from the structured interaction between its fundamental constituents, the neurons. Beyond the stimulated response by external perturbations, neurons present a background rest activity, as observed in both *in vivo* and *in vitro* experiments [1–4]. A natural question arises therefore about the relation between such two kinds of activity, spontaneous and stimulated. In particular, clarifying how the brain’s response to external stimuli can depend on the ongoing rest activity could shed light on the main mechanisms ruling the observed large variability in the dynamics [5]. An even more ambitious goal would be the prediction of the brain response to an external stimulus from the observation of the unperturbed rest signal [6,7]. This possibility is suggested by statistical mechanics and stochastic processes theory, whose framework allows one to derive the so-called fluctuation-dissipation relations (FDRs) [8]. They express the response function of a given variable to an external field in terms of unperturbed correlation functions of appropriate observables. In recent years, such relations have been extended beyond the realm of equilibrium systems to a very general class of models that exhibit nonequilibrium dynamics [9]. The problem of

forecasting the behavior of a system, and in particular its response to perturbations, from the study of the past history is a very general issue and has been addressed in many different physical contexts [8]. In biological systems, however, there are only a few cases where such a kind of approach has been attempted quantitatively. We can mention the study of evolution in bacteria reported in [10] and the application to the heart rate response [11]. More recently, in the context of brain dynamics, this framework has been applied to experimental magnetoencephalography (MEG) data of human brain activity [7] and to stochastic models for the dynamics of a single neuron [12]. In particular, in [7], in order to obtain an explicit form of the FDR to apply to data, the authors considered the celebrated Wilson-Cowan model for excitatory and inhibitory neuron populations [13,14]. In the linearized version of the model, exact expressions could be derived for response and correlation functions that were fitted to MEG data. The main result of this study confirmed that a prediction on the decay of the response function of brain activity from the observation of spontaneous fluctuations can be obtained, with good qualitative agreement between theory and experiments. Here we extend the analysis to a more general model that also allows one to consider imbalanced neuron populations and explore in more detail the different behaviors that can take place in the parameter space.

The Wilson-Cowan model considers a network of two populations of neurons, excitatory (E) and inhibitory (I), that

*lucilla.dearcangelis@unicampania.it

are coupled via four coefficients that represent the synaptic weights between E and I neurons (w_{EE} , w_{II} , w_{IE} , and w_{EI}). A neuron is activated by an input current, which takes into account the interaction with other neurons and an external field. The model can be studied at different levels of coarse graining, from the microscopic dynamics of the N single neurons, to the large-scale description which reduces to only two variables, namely, the fractions of active excitatory and inhibitory populations. In the large system size limit, one can derive two deterministic equations ruling the fixed points of the population dynamics and two coupled Langevin equations describing their fluctuations. In previous papers [15,16], this model was studied in the particular case of synaptic coefficients that depend on only the presynaptic neuron, namely, $w_{EI} = w_{II}$ and $w_{IE} = w_{EE}$, for both fully connected and sparse networks. The analysis in a 2D geometry is reported in [17]. For this choice of synaptic weights, the coupling matrix between excitatory and inhibitory populations takes a triangular form, implying an activity correlation function with a (double) exponential decay. Moreover, in [16] it was shown that a *bona fide* critical point can be identified for a specific value of the parameter $w_0 = w_{EE} - w_{II}$, characterized by a diverging characteristic time in the correlation function and by a power-law scaling of the activity avalanche distribution.

In this paper we study the fixed points and the correlation and response functions in the Wilson-Cowan model in the more general case where the above constraint on the synaptic strengths is released and considering different ratios of E and I neurons. This allows us to address the relevant issue related to the presence of an imbalance condition in the model. The important role played by the relative fraction of I neurons in the system behavior has been recently discussed for integrate and fire models in [18,19]. Previous results for specific values of the parameters (far from the critical point and in the presence of large external fields) have been reported in [20,21], where noisy limit cycles and quasicycles in the population dynamics were observed. See also the models discussed in [22–24]. Here we reconstruct the whole phase diagram for the total activity Σ and the imbalance between excitatory and inhibitory activity Δ (see below for the exact definition) in a region around the critical point identified in [16], in the limit of a vanishing external field. Our results unveil the existence of an abrupt, discontinuous change in the phase diagram, separating a region of finite activity from a region of almost zero activity. We then focus on the correlation and response functions, which show a rich phenomenology depending on the system parameters, featuring damped oscillations over several time regimes. Experimental studies of these quantities have been conducted, for instance, in neocortical slices, as reported in [25], or in rat somatosensory cortex cultures [26]. Other results can be found for correlations of alpha oscillations in [27] or for the activity fluctuations in cortical areas of the macaque monkey [28].

We then study the relation between correlation and response functions via the FDRs. In particular, the unperturbed state, described by Eq. (8) below, represents the spontaneous activity, while the stimulation is applied through a small perturbation to the initial condition, as detailed in Eqs. (15) and (23). In the case of a comparison with experimental data, a delicate issue can be represented by the correct modeling of

the applied stimulus, as discussed in [7], for instance, due to the kind of the specific stimulation. Finally, we compare the analytical solution of the linearized model to extensive numerical simulations of the microscopic dynamics and study the convergence towards the analytical predictions as a function of the system size [29]. Quite surprisingly, we find that, in some cases, such a convergence is very slow, requiring a huge number of neurons in the simulations.

The paper is organized as follows. In Sec. II we introduce the stochastic Wilson-Cowan model. In Sec. II A and II B we summarize the analytical results for correlation and response functions and provide details on the numerical simulations of the model, respectively. In Sec. III we discuss the fixed points of the dynamical equations, and in Sec. III A we comment on the eigenvalues that rule the dynamics. Then in Sec. IV and Sec. V we discuss the different behaviors observed in the model for correlation and response functions, respectively. Finally, in Sec. VI some conclusions are drawn. In the Appendix we provide details on the analytical computations.

II. THE STOCHASTIC WILSON-COWAN MODEL

The stochastic version of the Wilson-Cowan model [13,15,30] describes the coupled dynamics of a network of two populations, i.e., N_E excitatory and N_I inhibitory neurons, with χ_E and χ_I the fractions of excitatory (N_E/N) and inhibitory (N_I/N) neurons present in the network. Each neuron i in the model can be in two states, active ($a_i = 1$), i.e., a neuron firing an action potential or in its following refractory period, or quiescent ($a_i = 0$), i.e., a neuron at rest. The dynamics evolves according to a continuous time Markov process. The transition rate from active to quiescent state ($1 \rightarrow 0$) is α for all the neurons, while the rate from quiescent to active state ($0 \rightarrow 1$) depends on an activation function $f(S_i)$. Here S_i is the total synaptic input of the i th neuron, which is given by

$$S_i = \sum_j w_{ij} a_j + h_i, \quad (1)$$

where w_{ij} are the synaptic strengths and h_i is an external small field equal for all neurons ($h_i \equiv h = 10^{-6}$). In the present work the activation function is chosen to be

$$f(S) = \begin{cases} \beta \tanh(S), & S > 0, \\ 0, & S \leq 0. \end{cases} \quad (2)$$

In this study we set $\alpha = 0.1 \text{ ms}^{-1}$ and $\beta = 1 \text{ ms}^{-1}$ [16], and we consider full connectivity. The outgoing synaptic weights w_{ij} are defined as $\frac{w_{EE}}{N_E}$ for each excitatory to excitatory neuron, $-\frac{w_{EI}}{N_I}$ for inhibitory to excitatory, $\frac{w_{IE}}{N_E}$ for excitatory to inhibitory, and $-\frac{w_{II}}{N_I}$ for inhibitory to inhibitory connections. The input of a neuron, S_i , depends on only the type of neuron, namely, if the i th neuron is excitatory, then $S_i = S_E$, and if it is inhibitory, then $S_i = S_I$. Thus for our model

$$\begin{aligned} S_E &= \frac{w_{EE}}{N_E} k - \frac{w_{EI}}{N_I} l + h, \\ S_I &= \frac{w_{IE}}{N_E} k - \frac{w_{II}}{N_I} l + h, \end{aligned} \quad (3)$$

where k and l are the number of active excitatory and inhibitory neurons, respectively, evolving according to the

master equation [13]. In the Gaussian approximation, we can write

$$\begin{aligned} k &= N_E E + \sqrt{N_E} \xi_E, \\ l &= N_I I + \sqrt{N_I} \xi_I, \end{aligned} \quad (4)$$

where E and I are deterministic terms of the active excitatory and inhibitory population, which scale with the population size, and ξ_E and ξ_I are the stochastic fluctuation terms, which scale with the square root of the population size. It is then possible to expand the master equation as a Taylor series in (ξ_E, ξ_I) around the deterministic terms (E, I) , and, by retaining the two leading terms in the system size, one obtains the so-called linear noise approximation which provides two sets of coupled differential equations for (E, I) and (ξ_E, ξ_I) [30]. In order to more easily interpret the system behavior, it is convenient to introduce the variables $\Sigma = \chi_E E + \chi_I I$ and $\Delta = \chi_E E - \chi_I I$, which represent the total activity of the system and the imbalance in the activity between the excitatory and inhibitory population. The Wilson-Cowan equations for the deterministic terms (see the Appendix) are given by

$$\begin{aligned} \frac{d\Sigma}{dt} &= -\alpha \Sigma + [\chi_E f(S_E) + \chi_I f(S_I)] \\ &\quad - \Sigma \frac{[f(S_E) + f(S_I)]}{2} - \Delta \frac{[f(S_E) - f(S_I)]}{2}, \\ \frac{d\Delta}{dt} &= -\alpha \Delta + [\chi_E f(S_E) - \chi_I f(S_I)] \\ &\quad - \Sigma \frac{[f(S_E) - f(S_I)]}{2} - \Delta \frac{[f(S_E) + f(S_I)]}{2}, \end{aligned} \quad (5)$$

where the input currents are written as

$$\begin{aligned} S_E &= w_{EE} E - w_{EI} I + h, \\ S_I &= w_{IE} E - w_{II} I + h, \end{aligned} \quad (6)$$

and the dynamical equations for E and I are

$$\begin{aligned} \frac{dE}{dt} &= -\alpha E + (1 - E)f(S_E), \\ \frac{dI}{dt} &= -\alpha I + (1 - I)f(S_I). \end{aligned} \quad (7)$$

Conversely, the linearized Langevin equations for the fluctuating variables can be expressed as [15,16,20,29] (see also the Appendix)

$$\frac{d}{dt} \begin{pmatrix} \xi_\Sigma \\ \xi_\Delta \end{pmatrix} = \mathbf{A} \begin{pmatrix} \xi_\Sigma \\ \xi_\Delta \end{pmatrix} + \mathbf{D} \begin{pmatrix} \eta_\Sigma \\ \eta_\Delta \end{pmatrix}, \quad (8)$$

where the coefficients of \mathbf{A} are calculated using the stationary solutions of Eq. (5) and \mathbf{D} is the amplitude matrix of the independent white-noise variables η_Σ and η_Δ , which satisfy $\langle \eta_i(t) \rangle = 0$ and $\langle \eta_i(t) \eta_j(t') \rangle = \delta_{ij} \delta(t - t')$. A similar two-variable model also has been introduced in the context of moderately dense fluids to study the dynamics of a massive tracer [31,32]. The details of the calculations and the coefficients of the matrix \mathbf{A} and \mathbf{D} are given in the Appendix. Notice that so far no hypothesis is made for the value of the w 's.

A. Correlation and response functions

The correlation matrix for the Eq. (8) in the stationary state can be written as [31]

$$C_{ij}(t) \equiv \langle \xi_i(t) \xi_j(0) \rangle = (e^{\mathbf{A}t} \boldsymbol{\sigma})_{ij}, \quad (9)$$

where angular brackets $\langle \dots \rangle$ denote average over noise, $(i, j) = (\Sigma, \Delta)$, $\boldsymbol{\sigma}$ is the covariance matrix, and $t \geq 0$. The correlation functions are

$$\begin{aligned} C_{\Sigma\Sigma}(t) &= \frac{1}{\sqrt{-\Theta}} \{ [(x - \lambda_2)\sigma_{11} + y\sigma_{21}]e^{\lambda_1 t} \\ &\quad - [(x - \lambda_1)\sigma_{11} + y\sigma_{21}]e^{\lambda_2 t} \}, \end{aligned} \quad (10)$$

$$\begin{aligned} C_{\Sigma\Delta}(t) &= \frac{1}{\sqrt{-\Theta}} \{ [(x - \lambda_2)\sigma_{12} + y\sigma_{22}]e^{\lambda_1 t} \\ &\quad - [(x - \lambda_1)\sigma_{12} + y\sigma_{22}]e^{\lambda_2 t} \}, \end{aligned} \quad (11)$$

$$\begin{aligned} C_{\Delta\Sigma}(t) &= \frac{1}{\sqrt{-\Theta}} \{ [z\sigma_{11} - (x - \lambda_1)\sigma_{21}]e^{\lambda_1 t} \\ &\quad - [z\sigma_{11} - (x - \lambda_2)\sigma_{21}]e^{\lambda_2 t} \}, \end{aligned} \quad (12)$$

$$\begin{aligned} C_{\Delta\Delta}(t) &= \frac{1}{\sqrt{-\Theta}} \{ [z\sigma_{12} - (x - \lambda_1)\sigma_{22}]e^{\lambda_1 t} \\ &\quad - [z\sigma_{12} - (x - \lambda_2)\sigma_{22}]e^{\lambda_2 t} \}, \end{aligned} \quad (13)$$

where $\lambda_{1,2}$ are the eigenvalues of the matrix \mathbf{A} , x, y, z , and w its coefficients, which are functions of the model parameters, and $\sqrt{-\Theta} = \sqrt{(x - w)^2 + 4yz}$ (see the Appendix). The behavior of the correlation functions is a double exponential decay with characteristic times $\tau_1 = 1/\lambda_1$ and $\tau_2 = 1/\lambda_2$. In case of complex eigenvalues, i.e., $\lambda_1 = a + ib$, $\lambda_2 = a - ib$, where $a = (x + w)/2$ and $ib = \sqrt{-\Theta}/2$, the correlation functions show oscillatory behavior with frequency b :

$$\begin{aligned} C_{\Sigma\Sigma}(t) &= \sigma_{11} e^{at} \cos(bt) + \frac{(x - a)\sigma_{11} + y\sigma_{21}}{b} e^{at} \sin(bt), \\ C_{\Sigma\Delta}(t) &= \sigma_{12} e^{at} \cos(bt) + \frac{(x - a)\sigma_{12} + y\sigma_{22}}{b} e^{at} \sin(bt), \\ C_{\Delta\Sigma}(t) &= \sigma_{21} e^{at} \cos(bt) + \frac{z\sigma_{11} - (x - a)\sigma_{21}}{b} e^{at} \sin(bt), \\ C_{\Delta\Delta}(t) &= \sigma_{22} e^{at} \cos(bt) + \frac{z\sigma_{12} - (x - a)\sigma_{22}}{b} e^{at} \sin(bt), \end{aligned} \quad (14)$$

with $a < 0$. The linearization around the fixed points is valid only for values of the parameters for which the matrix \mathbf{A} has stable eigenvalues.

We next evaluate the linear response function of the system to an instantaneous weak perturbation, defined as

$$R_{ij}(t) \equiv \frac{\overline{\delta \xi_i(t)}}{\delta \xi_j(0)}, \quad (15)$$

where $(i, j) = (\Sigma, \Delta)$. Equation (15) represents the average response of $\xi_i(t)$ at time t to the applied pulse perturbation on the variable $\xi_j(0)$ at time $t = 0$. The symbol $\overline{(\dots)}$ denotes the nonstationary average over the trajectories. The response matrix of the system can be calculated for $t > 0$ as

$$\mathbf{R}(t) = e^{\mathbf{A}t}. \quad (16)$$

From Eqs. (9) and (16) we can obtain the FDRs which connect the linear response to the spontaneous fluctuations [7] as

$$\mathbf{R}(t) = \mathbf{C}(t)\sigma^{-1}. \quad (17)$$

The response functions for the small perturbations expressed in terms of Σ and Δ are therefore

$$\begin{aligned} R_{\Sigma\Sigma}(t) &= (\sigma^{-1})_{11}C_{\Sigma\Sigma}(t) + (\sigma^{-1})_{21}C_{\Sigma\Delta}(t), \\ R_{\Sigma\Delta}(t) &= (\sigma^{-1})_{12}C_{\Sigma\Sigma}(t) + (\sigma^{-1})_{22}C_{\Sigma\Delta}(t), \\ R_{\Delta\Sigma}(t) &= (\sigma^{-1})_{11}C_{\Delta\Sigma}(t) + (\sigma^{-1})_{21}C_{\Delta\Delta}(t), \\ R_{\Delta\Delta}(t) &= (\sigma^{-1})_{12}C_{\Delta\Sigma}(t) + (\sigma^{-1})_{22}C_{\Delta\Delta}(t), \end{aligned} \quad (18)$$

where the exact form of the covariance matrix σ is given in the Appendix. From Eq. (18), we see that both the autocorrelations and the cross correlations are required to calculate the response to a weak instantaneous perturbation.

In Ref. [7] the model was applied to describe MEG data of human brains of healthy subjects. It was shown that correlation and response functions could be well fitted by the model, with parameters corresponding to the case of the balance condition. In particular, correlation functions show double exponential decay, while response functions are well described by a single exponential decay.

B. Numerical simulation methods

The continuous time Markov process that describes the dynamics of the system can be efficiently simulated by the Gillespie algorithm [33], which we describe here for completeness. The configuration of the system at a given time t is completely determined by the number of active excitatory neurons k and the number of active inhibitory neurons l . Given k and l at time t , we compute the synaptic inputs S_E and S_I from Eq. (3), and then the activation (a) and deactivation (d) rates for excitatory (e) and inhibitory (i) neurons, which are given by

$$\begin{aligned} r_{de} &= \alpha k, \\ r_{di} &= \alpha l, \\ r_{ae} &= (N_E - k)f(S_E), \\ r_{ai} &= (N_I - l)f(S_I), \end{aligned} \quad (19)$$

and the total rate $r_{\text{tot}} = r_{de} + r_{di} + r_{ae} + r_{ai}$. As the process is Markovian, the time interval to the next event is extracted from an exponential distribution, $P(\Delta t) = r_{\text{tot}} \exp(-r_{\text{tot}}\Delta t)$, and the event is selected among de , di , ae , and ai with probability $\frac{r_{de}}{r_{\text{tot}}}$, $\frac{r_{di}}{r_{\text{tot}}}$, $\frac{r_{ae}}{r_{\text{tot}}}$, $\frac{r_{ai}}{r_{\text{tot}}}$, respectively. Then the time is incremented by Δt and the selected event is performed increasing by one, or decreasing by one, the number of active neurons k or l .

Because in the Gillespie algorithm the time step Δt is proportional to N^{-1} , for a very large number of neurons the simulation becomes very inefficient. In this case one can simulate the model using the nonlinear Langevin equations

$$\begin{aligned} \frac{dk}{dt} &= -\alpha k + (N_E - k)f(S_E) + \sqrt{\alpha k + (N_E - k)f(S_E)}\eta_E(t), \\ \frac{dl}{dt} &= -\alpha l + (N_I - l)f(S_I) \\ &\quad + \sqrt{\alpha l + (N_I - l)f(S_I)}\eta_I(t), \end{aligned} \quad (20)$$

with a fixed time step. The nonlinear equations are equivalent to the full master equation (Gillespie algorithm), provided that the time step of integration is small enough and the number of neurons is not too small [16]. Here we used a time step of $\Delta t = 10^{-3}$ ms. Data for correlation and response functions are averaged over about 10^7 realizations.

After an appropriate time interval, the process reaches stationarity, so that k and l fluctuate around their mean values $\bar{k} = N_E \bar{E}$ and $\bar{l} = N_I \bar{I}$, where \bar{E} and \bar{I} are the time average value of the deterministic components. At stationarity, the fluctuations can be computed by

$$\begin{aligned} \xi_E(t) &= N_E^{-1/2}(k - \bar{k}), \\ \xi_I(t) &= N_I^{-1/2}(l - \bar{l}), \end{aligned} \quad (21)$$

and

$$\begin{aligned} \xi_\Sigma(t) &= \chi_E \xi_E(t) + \chi_I \xi_I(t), \\ \xi_\Delta(t) &= \chi_E \xi_E(t) - \chi_I \xi_I(t). \end{aligned} \quad (22)$$

In this way it is possible to compute the auto-correlations and cross-correlations $C_{\Sigma\Sigma}(t)$, $C_{\Sigma\Delta}(t)$, $C_{\Delta\Sigma}(t)$, and $C_{\Delta\Delta}(t)$ from Eq. (9).

We next evaluate the response function matrix $\mathbf{R}(t)$ using the following procedure. To compute $R_{\Sigma\Sigma}(t)$ and $R_{\Delta\Sigma}(t)$, after the process has reached stationarity, at a given time t' , k and l are perturbed in such a way that

$$\begin{aligned} \xi_\Sigma(t') &\rightarrow \xi_\Sigma(t') + \epsilon, \\ \xi_\Delta(t') &\rightarrow \xi_\Delta(t'), \end{aligned} \quad (23)$$

where ϵ is a small quantity. This is performed by increasing k by $\frac{\sqrt{N_E}}{2\chi_E}\epsilon$, and l by $\frac{\sqrt{N_I}}{2\chi_I}\epsilon$. Then we compute

$$\begin{aligned} R_{\Sigma\Sigma}(t) &= \epsilon^{-1} \langle \xi_\Sigma(t' + t) \rangle, \\ R_{\Delta\Sigma}(t) &= \epsilon^{-1} \langle \xi_\Delta(t' + t) \rangle, \end{aligned} \quad (24)$$

where the average $\langle \dots \rangle$ is done on the realization of the noise, and on different starting configurations at time t' . To compute $R_{\Sigma\Delta}(t)$ and $R_{\Delta\Delta}(t)$ we use a similar procedure, with the difference that we increase $\xi_\Delta(t')$ instead of $\xi_\Sigma(t')$. In this case one has to increase k by $\frac{\sqrt{N_E}}{2\chi_E}\epsilon$ and decrease l by $\frac{\sqrt{N_I}}{2\chi_I}\epsilon$.

III. FIXED POINTS

In previous studies, usually synaptic strengths are assumed to solely depend on the type of presynaptic neuron, namely, $w_{EI} = w_{II}$ and $w_{IE} = w_{EE}$. Following this assumption, the matrix \mathbf{A} has an upper triangular form, and the fixed point for imbalance in activity is $\Delta^* = 0$. Therefore the previous condition on synaptic strengths sets the system in a state realizing the balance of excitatory and inhibitory activity, which leads to the presence of a critical point at a specific value of $w_0 = w_{EE} - w_{II} = \alpha/\beta = 0.1$, where also Σ tends to vanish [16]. In the present study, we focus on the behavior of the system following the removal of such hypothesis, namely, by slowly driving it out of the balance of excitation and inhibition. We start by fixing the values of the strengths $w_{EE} = 6.95$ and $w_{II} = 6.85$, setting the system at criticality. We then define $w_{EI} = w_{II} + \delta EI$ and $w_{IE} = w_{EE} + \delta IE$, where δEI and δIE are the two control parameters tuning

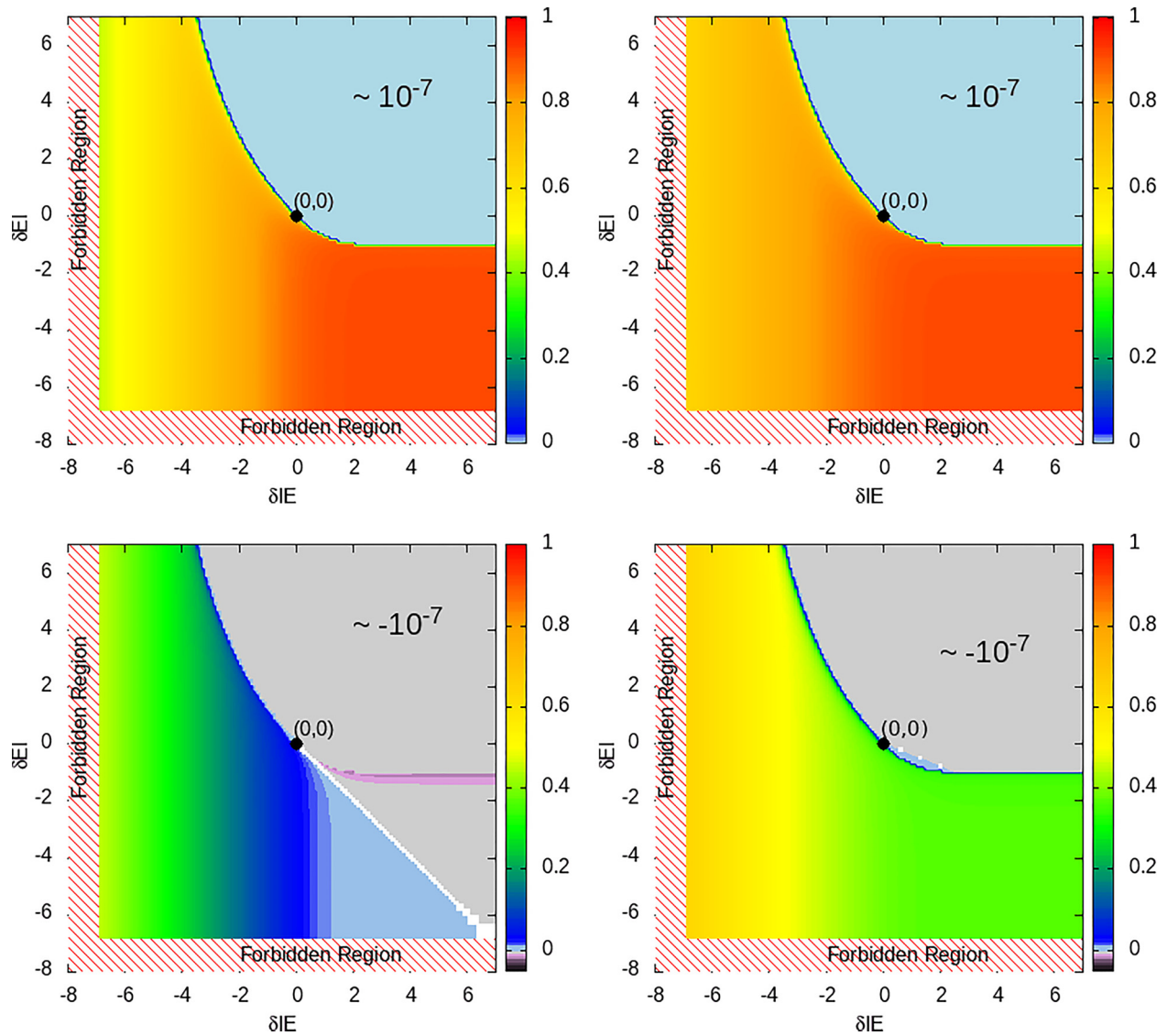


FIG. 1. Values of Σ_0 (top) and Δ_0 (bottom), solutions of Eq. (5), as function of the parameters measuring the variation in the synaptic strengths. The left column refers to $\chi_E = \chi_I = 50\%$, and the right column is for $\chi_E = 70\%$ and $\chi_I = 30\%$. The parameter values for all calculations are $w_{EE} = 6.95$, $w_{II} = 6.85$, $h = 10^{-6}$, $\alpha = 0.1$, $w_{EI} = w_{II} + \delta EI$, and $w_{IE} = w_{EE} + \delta IE$. The forbidden regions correspond to the parameter range where w_{IE} or w_{EI} become negative.

the imbalance condition. Structural inhibition is also tuned by analyzing systems with different fractions of inhibitory neurons, i.e., $\chi_E = \chi_I = 50\%$ and $\chi_E = 70\%$, $\chi_I = 30\%$. We numerically solve the deterministic Eqs. (5) using Newton’s method for fixed point analysis for different values of δEI and δIE , in a range corresponding to positive synaptic connections, to derive the values of Σ_0 and Δ_0 at the fixed point (Fig. 1).

The activity Σ_0 for $(\chi_E = \chi_I = 50\%)$ and for $(\chi_E = 70\%, \chi_I = 30\%)$ shows similar behaviors. In the regime where δEI is negative, if we change δIE from positive to negative values, the activity Σ_0 initially shows a plateau near one and then gradually decreases to 50% of its initial value. On the other hand, if we change δEI keeping δIE fixed, the activity Σ_0 is almost constant up to certain values of δEI where the activity drops drastically to a very small value ($\sim 10^{-7}$), as shown in Fig. 1, giving rise to a boomerang-like

transition line from a finite to a very small activity. For a system with $\chi_E = 70\%$ and $\chi_I = 30\%$ the activity Σ_0 shows a similar behavior, with small discrepancies with respect to the system with $\chi_E = \chi_I = 50\%$ for very negative δIE . This behavior can be understood by considering the different role of the perturbations in the dynamics: A large variation δIE implies that the synaptic connections from the excitatory to the inhibitory population are stronger than in the case of balanced activity, leading to an increased activity of the inhibitory population. Conversely, large δEIs imply that the inhibitory population strongly hampers the activity of the excitatory one. As a consequence, the system activity stems from the interplay between the relative role of the two populations. The observation that the excitability of the system strongly increases below the bisector $\delta IE = -\delta EI$ suggests that the imbalance in excitation is mostly controlled by the inhibitory population, whose activity cannot compensate the excitatory one either

because of its weak connections (δEI is too small) or because they are weakly stimulated by the excitatory population (δIE is too small). Interestingly, in the first quadrant the δ 's are both positive, which allows balance to be achieved within a wide range of parameters.

Conversely, a more clear sensitivity to parameters is observed for the imbalance Δ_0 at the fixed point. For systems with equal-size populations ($\chi_E = \chi_I = 50\%$), if we progressively decrease δIE , keeping $\delta EI \leq 0$ fixed, the imbalance Δ_0 starts from a very small negative value ($\sim -10^{-7}$), vanishes at the bisector line $\delta IE = -\delta EI$, and gradually increases to a maximum value of ~ 0.5 . Conversely, if we change δEI , keeping $\delta IE \geq 0$ fixed, Δ_0 appears to be roughly independent of δEI but abruptly drops to a very small negative value ($\sim -10^{-7}$) for parameter values above the bisector line. Activity therefore appears imbalanced in favor of excitation in a wide region of parameters corresponding to large positive Σ_0 . The only difference with systems with a lower percentage of inhibitory neurons ($\chi_E = 70\%$, $\chi_I = 30\%$) is that positive Δ_0 are also observed in the fourth quadrant for small values of δEI . This behavior can be attributed to the different size of the two populations, since for the same δ values the inhibitory activity is not sufficient to balance the excitatory one. Data confirm that for very small δIE the system is always imbalanced in favor of excitation (supercritical behavior), whereas inhibition slightly overcomes excitation (subcritical behavior) in the first quadrant parameter region. Finally, we observe that, as the deterministic solutions from Eq. (7) for E_0 and I_0 are independent of the population size, the value of Δ_0 for ($\chi_E = \chi_I = 50\%$) always should be smaller than that for ($\chi_E = 70\%$, $\chi_I = 30\%$).

A. Eigenvalues

Next, we calculate the eigenvalues for different values of δEI and δIE . We stress that, under the hypothesis that synaptic connections solely depend on the presynaptic neuron, the matrix \mathbf{A} always has real eigenvalues, corresponding to the two inverse characteristic times in the correlation functions. In the present, more general case the eigenvalues can become complex. In Fig. 2 (top left) we show in different colors the parameter regions where eigenvalues are real (cyan region) and complex (red region). The eigenvalues are independent of the size of the excitatory or inhibitory populations (see Sec. II) and have a nonzero imaginary part in two regions of the parameter space. In the diagonal region along the $\delta EI = -\delta IE$ line the imaginary part of the eigenvalues is very small, close to zero. Conversely, in the horizontal region the imaginary part can assume a wide range of values, mainly depending on δIE (Fig. 2, top right). Figure 2 (bottom) shows the real part of the eigenvalues λ_1 and λ_2 . The eigenvalues are all negative, indicating that the system is stable for any value of the parameters inside this region of the parameter space: we computed the long-time limit of Eq. (5), which therefore brings the system to an attractive fixed point. In the first quadrant, corresponding to $\Sigma_0 \simeq 0$ and $\Delta_0 \simeq 0$, the real part of the eigenvalue λ_1 becomes constant and close to zero whereas λ_2 exhibits large negative values. In the rest of the parameter space, whereas λ_1 assumes almost constant values, λ_2 appears to depend solely on the parameter δIE , becoming

more negative for decreasing synaptic strengths. We will now evaluate the correlation functions and the corresponding response functions at different locations of the parameter space (points A to G).

IV. CORRELATION FUNCTIONS

We analyze next the auto-correlation and cross-correlation functions at the points reported in the parameter space (Fig. 2) by analytical calculation of Eqs. (10)–(14). The correlation functions show (Fig. 3) either a double exponential decay or oscillations depending on whether the eigenvalues are real or complex. Indeed, oscillations are observed at points B and C, with a frequency given by the absolute value of the imaginary part of the eigenvalue and independent of the population size. Interestingly, the frequency, evaluated for different δEI , scales with δIE with an exponent smaller than one (see inset of Fig. 3), confirming the important role of the activity of the inhibitory population in the system dynamics. Moreover, we observe that for systems with equal populations ($\chi_E = \chi_I = 50\%$), there are strong phase differences and large amplitude differences between the self- and cross-correlation functions, which for the system with $\chi_E = 70\%$, $\chi_I = 30\%$ (values typical of mammalian brains) is almost absent (see points A and B). On the other hand, for real eigenvalues, the analytical solution provides correlation functions which are a double exponential with characteristic times which do not depend on the population size. For instance, the fitting procedure gives $\tau_1 = 0.92$ and $\tau_2 = 0.23$ at point G. Interestingly, in the first quadrant the exponential containing the eigenvalue λ_1 has an amplitude close to zero ($\simeq 10^{-8}$); therefore the correlation functions all exhibit a sharp single exponential decay.

Next, we compare our analytical data with the data obtained from simulations of the Wilson-Cowan model using the Gillespie algorithm, or the nonlinear Langevin equations when the number of neurons is large. Figure 4 shows the plots of the auto- and cross-correlation functions obtained from numerical simulations and analytical predictions for equal population systems at all the points shown in the parameter space in Fig. 2. We find that the analytical predictions are perfectly matching with the simulated data, provided that the number of neurons used in simulations is large enough. Namely, simulations must be performed with a total number of neurons $N > \bar{\Sigma}^{-2}$, where $\bar{\Sigma}$ is the mean value of the activity. Indeed, fluctuations in the activity are of order $N^{1/2}$, and the linear approximation (8) is valid only when fluctuations are smaller than the mean values. This is particularly relevant at points in phase space where the mean value $\bar{\Sigma}$ is very low, for example, at point C of Fig. 2 where the mean value is $\bar{\Sigma} \sim 10^{-7}$. In Fig. 5 we show the autocorrelation $C_{\Sigma\Sigma}(t)$ at point C for different number of neurons N . We see a strong dependence of the results on N up to $N \sim 10^{14}$.

The correlation functions evaluated at all the different points marked in the parameter space are shown in Fig. 6. One observes high-frequency oscillations for $\delta EI = -0.5$ and $\delta IE = +4$ (point C), for all correlation functions, for both the considered fractions of excitatory and inhibitory populations. The other points D, E, and F show a simple exponential decay for the auto-correlations of Σ and Δ , while cross-correlations

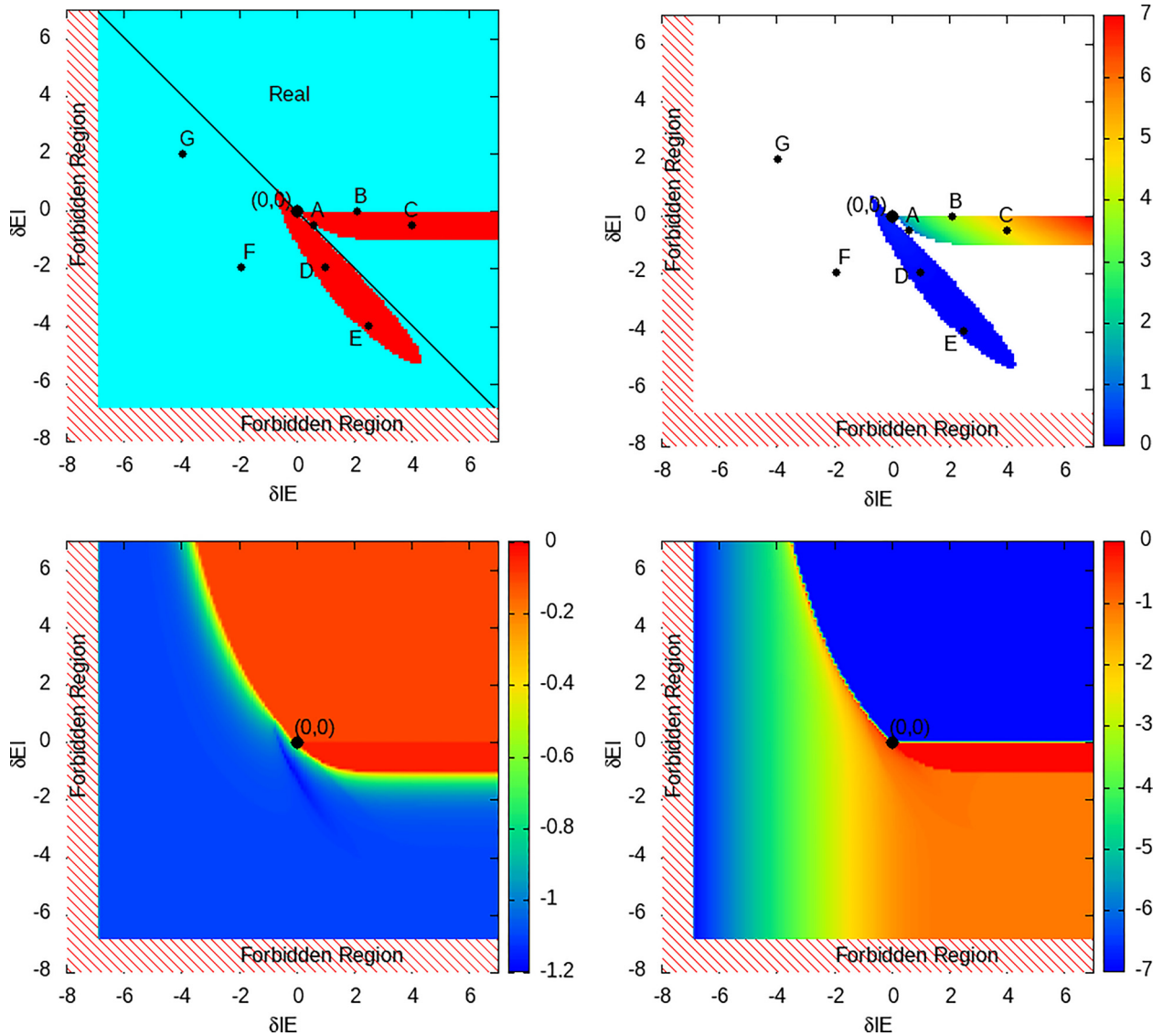


FIG. 2. (Top left) Eigenvalue phase diagram for different imbalance in synaptic strengths. Cyan identifies the region with real eigenvalues, whereas red indicates the region where eigenvalues are complex. (Top right) The values of the imaginary part of the eigenvalues. Letters identify the points in the phase diagram for which correlation and response functions have been evaluated. (Bottom left and right) The values of the real part of the eigenvalues λ_1 and λ_2 , respectively. The forbidden regions correspond to the parameter range where w_{IE} or w_{EI} become negative. Eigenvalues are independent of the population size. The numerical parameter values for all the calculations are $w_{EE} = 6.95$, $w_{II} = 6.85$, $h = 10^{-6}$, $\alpha = 0.1$, $w_{EI} = w_{II} + \delta EI$, and $w_{IE} = w_{EE} + \delta IE$.

are characterized by nonmonotonic behavior, featuring also a negative region for $C_{\Delta\Sigma}$ in the case of equal fraction populations. This phenomenon, pronounced in cases D and E, can be interpreted as a “backscattering” in Δ activity, namely, a negative fluctuation of Δ that follows a positive fluctuation of Σ after a certain time.

V. RESPONSE FUNCTIONS

We next calculate the response of the system to small instantaneous perturbations according to Eq. (18). Figure 7 shows the four different response functions for equal population systems. Under the hypothesis of synaptic strengths

depending solely on the presynaptic neuron type, previous calculations [7] have shown that, due to the upper triangular form of the coupling matrix \mathbf{A} , the response function exhibits a simple exponential decay behavior ($R_{\Sigma\Sigma}$ and $R_{\Delta\Delta}$), a double exponential decay ($R_{\Sigma\Delta}$), or it vanishes ($R_{\Delta\Sigma}$). The single exponential stems from the fact that the cross-correlation term cancels out one exponential decay. In the imbalanced case, the response functions show a more complex behavior, with oscillations at the points in parameter space where eigenvalues are complex.

To obtain the response function from simulations, and therefore compare analytical prediction to numerical data, we apply a weak perturbation to the system in order to remain

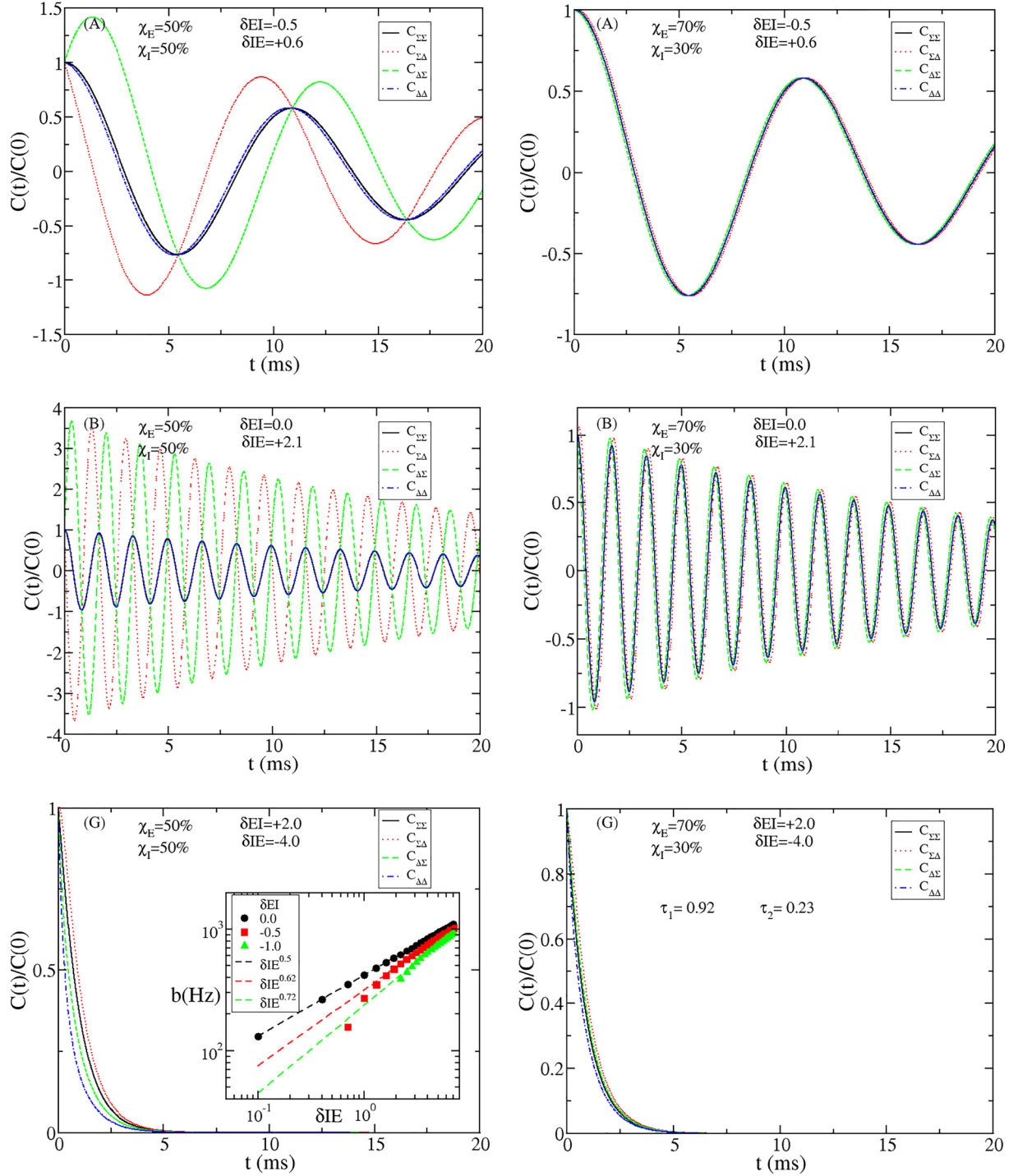


FIG. 3. The correlation functions evaluated at the different points A, B, G in the eigenvalue phase diagram (Fig. 2). The left column is for $\chi_E = \chi_I = 50\%$, and the right column is for $\chi_E = 70\%$ and $\chi_I = 30\%$. The inset shows the oscillation frequency b as function of δIE for different values of δEI . The parameter values used for the solution of Eqs. (5) are $w_{EE} = 6.95$, $w_{II} = 6.85$, $h = 10^{-6}$, $\alpha = 0.1$, $w_{EI} = w_{II} + \delta EI$, and $w_{IE} = w_{EE} + \delta IE$. Time is measured in ms.

in the linear regime. We take an equilibrium configuration, namely, a configuration at stationarity: we increase the value of ξ_Σ or ξ_Δ by a small amount ϵ and compute $\epsilon^{-1}\langle \xi_\Sigma(t) \rangle$ or $\epsilon^{-1}\langle \xi_\Delta(t) \rangle$, respectively, at subsequent times, as described in Sec. II B. Figure 7 shows the comparison of the response functions between analytical calculation and simulation data for all the points shown in the eigenvalue phase diagram Fig. 2. The

symbols represent the simulation data, and the solid lines the data obtained from the analytical calculations of the response functions using Eq. (18). As in the case of correlations, numerical data and analytical calculations match well provided the number of neurons is large enough. Moreover, in this case a small value of ϵ has to be chosen: data in Fig. 7 were obtained with $\epsilon = 10^{-3}$.

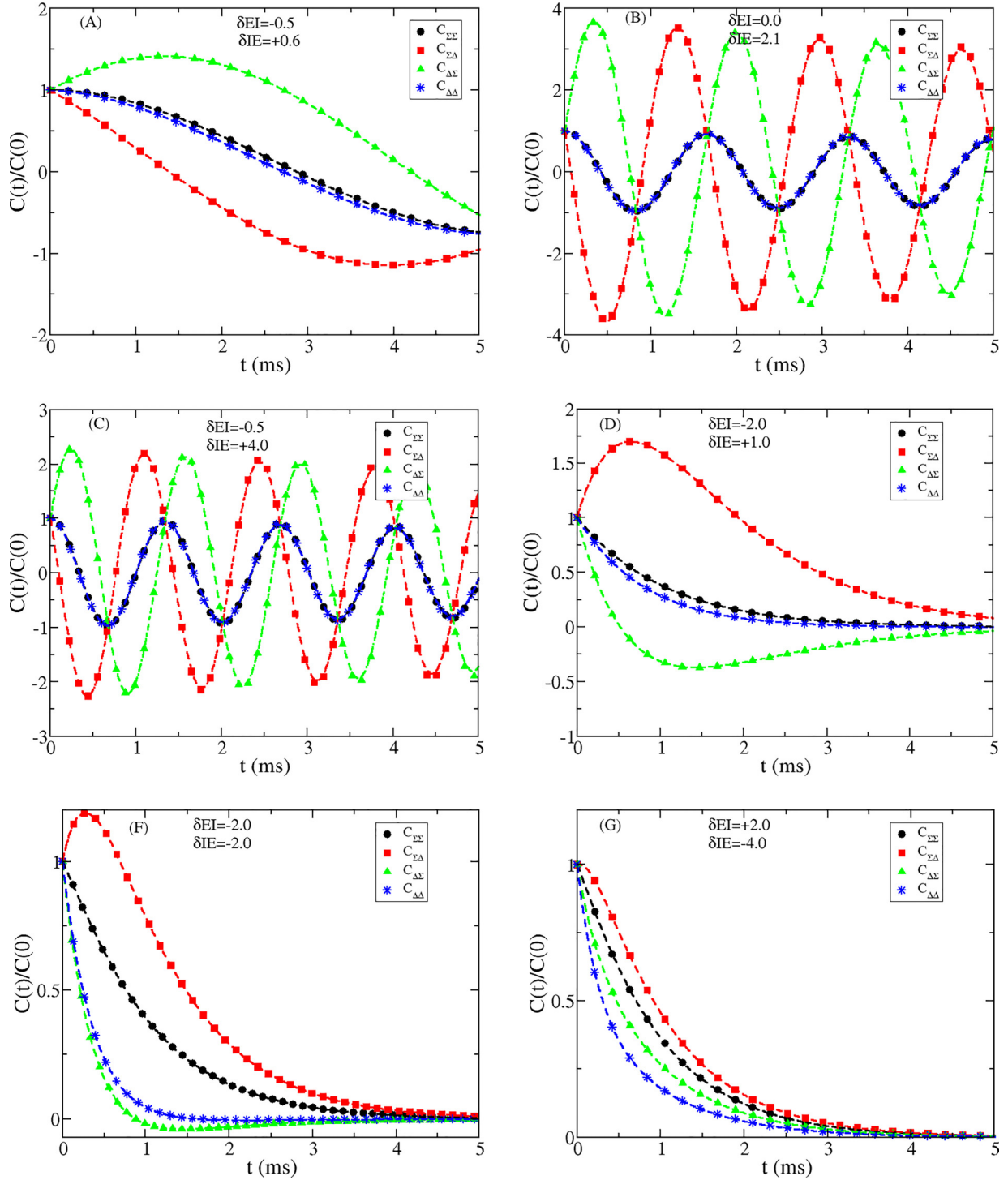


FIG. 4. The correlation functions for $\chi_E = \chi_I = 50\%$ evaluated at different points A, B, C, D, F, and G in the phase diagram (Fig. 2). The symbols are the results of simulations with $N = 10^{14}$ neurons, with parameters $w_{EE} = 6.95$, $w_{II} = 6.85$, $h = 10^{-6}$, $\alpha = 0.1$, $w_{EI} = w_{II} + \delta EI$, and $w_{IE} = w_{EE} + \delta IE$, whereas dashed lines represent analytical results. Details of simulations are reported in Sec. II B.

VI. CONCLUSIONS

Each neuron in the brain can receive thousands of excitatory and inhibitory synaptic inputs. In physiological conditions, the ratio of excitatory to inhibitory inputs remains stable at both single-cell and global circuit levels, a property called balance of excitation and inhibition (EI) [34,35].

Although the existence of EI balance in the mammalian cortex has been widely studied and its disruption has been implicated in many brain diseases affecting higher cognitive functions, it is not yet clear how this balance is maintained in healthy brains [36,37]. Experimentally, imbalance arises hampering excitatory or inhibitory neurotransmission with selected antagonists [38]. In neuronal networks, imbalance

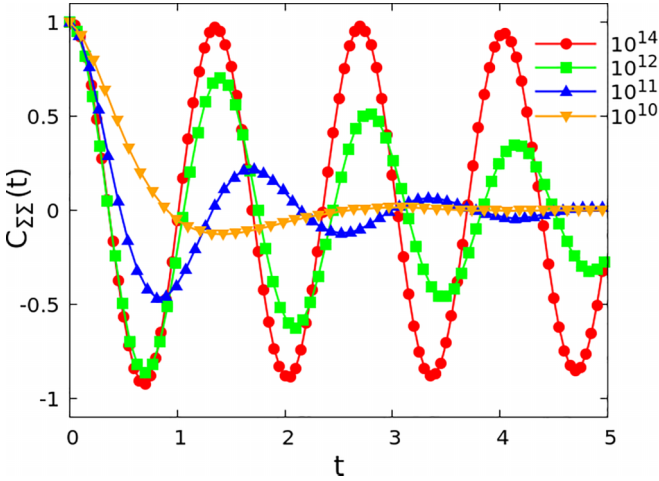


FIG. 5. The correlation function $C_{\Sigma\Sigma}(t)$ for $\chi_E = \chi_I = 50\%$ evaluated at point C in the phase diagram (Fig. 2), for a different number of neurons $N = 10^{10}, 10^{11}, 10^{12}, 10^{14}$, with parameters $w_{EE} = 6.95, w_{II} = 6.85, h = 10^{-6}, \alpha = 0.1, w_{EI} = w_{II} + \delta EI$, and $w_{IE} = w_{EE} + \delta IE$. Details of simulations are reported in Sec. II B.

is obtained controlling the percentage of inhibitory synapses, the connectivity network, or the neuron excitability and can lead to an excess of large bursts, as observed in epileptic systems. Several experimental and theoretical studies have confirmed that imbalanced conditions alter spontaneous brain activity. Imbalance modifies the typical scale-free behavior of activity in the resting state [38,39] and its temporal features [40,41]. Analogously, EI balance and imbalance may affect the relation between spontaneous and evoked activity, i.e., the response to external stimuli [5]. Recently, the problem has been addressed theoretically by means of the FDRs connecting the spontaneous fluctuations of a system with the response function to external perturbations [7]. The analytical derivation, based on the linear noise approximation of the Wilson-Cowan model, on the main assumption of EI balance provides a double exponential decay for the correlation functions and a simple exponential for the $R_{\Sigma\Sigma}$. In this study we investigated its extension to imbalanced conditions in a wide range of parameters tuning such imbalance.

Results indicate that the main parameter controlling activity in imbalance is δIE , namely, the variation in the synaptic strength exciting the inhibitory population. Conversely, the other parameter δEI , expressing the strength of inhibition received by the excitatory neurons, appears to have a different role: It controls the transition from a high-activity regime to a regime (in the first quadrant) where $\Sigma_0 \sim \Delta_0 \sim 0$, as well as the transition from real to complex eigenvalues. The overall behavior of the system stems from the interplay between these two independent effects. The presence of complex eigenvalues leads to a novel oscillatory behavior for the correlation functions in a narrow range of δEI and, consequently, oscillations in the response functions, with a frequency depending on the parameter δIE . The important remark is that analytical results are fully confirmed by Gillespie simulations of Wilson-Cowan networks in the limit of very large system size. Indeed, this limit, implemented to derive the FDRs, results in being extremely stringent since full agreement with simulation data is achieved for systems as large as $N \sim 10^{14}$ neurons.

Interestingly, the FDRs are fulfilled numerically even for smaller system sizes, where the agreement with the analytical solution is not perfect. The present results, obtained for a population model, are also in good agreement with simulations of integrate and fire networks models [18], where oscillations in the correlation functions were observed in the supercritical regime and the frequency depended on the percentage of inhibitory neurons and their level of connectivity.

ACKNOWLEDGMENTS

L.d.A. and A.d.C. would like to thank MIUR Project No. PRIN2017WZFTZP for financial support. A.S. acknowledges support from MIUR Project No. PRIN201798CZLJ. H.J.H. thanks the University of Campania for the visiting professorship and FUNCAP for financial support. Work supported by #NEXTGENERATIONEU (NGEU) and funded by the Ministry of University and Research (MUR), National Recovery and Resilience Plan (NRRP), project MNESYS (PE0000006) – A Multiscale integrated approach to the study of the nervous system in health and disease (DN. 1553 11.10.2022).

APPENDIX

1. Stochastic Wilson-Cowan model

We present here the derivation of the Wilson-Cowan equations in the general case where no assumption is made on the synaptic strengths and the neuronal populations can have different sizes. The dynamics evolves according to a master equation for the probability $p_{k,l}(t)$, where the number of active excitatory and active inhibitory neurons is k and l . We set

$$\begin{aligned} k &= N_E E + N_E^{1/2} \xi_E, \\ l &= N_I I + N_I^{1/2} \xi_I. \end{aligned} \quad (\text{A1})$$

The input currents are

$$\begin{aligned} S_E &= \frac{w_{EE}k}{N_E} - \frac{w_{EI}l}{N_I} + h_E, \\ S_I &= \frac{w_{IE}k}{N_E} - \frac{w_{II}l}{N_I} + h_I. \end{aligned} \quad (\text{A2})$$

The master equation, describing the evolution of the probabilities $p_{k,l}(t)$ that the system is in the state (k, l) at time t , is

$$\begin{aligned} \frac{dp_{k,l}(t)}{dt} &= \alpha[(k+1)p_{k+1,l}(t) - kp_{k,l}(t)] \\ &\quad + \{(N_E - k + 1)f[S_E(k-1, l)]p_{k-1,l}(t) \\ &\quad - (N_E - k)f[S_E(k, l)]p_{k,l}(t)\} \\ &\quad + \alpha[l+1)p_{k,l+1}(t) - lp_{k,l}(t)] \\ &\quad + \{(N_I - l + 1)f[S_I(k, l-1)]p_{k,l-1}(t) \\ &\quad - (N_I - l)f[S_I(k, l)]p_{k,l}(t)\}. \end{aligned} \quad (\text{A3})$$

Now using $e^{\partial_k} \{kp_{k,l}(t)\} = (k+1)p_{k+1,l}(t)$, we have

$$\begin{aligned} \frac{dp_{k,l}(t)}{dt} &= \alpha(e^{\partial_k} - 1)kp_{k,l}(t) + (e^{-\partial_k} - 1)\{(N_E - k) \\ &\quad \times f[S_E(k, l)]p_{k,l}(t)\} + \alpha(e^{\partial_l} - 1)lp_{k,l}(t) \\ &\quad + (e^{-\partial_l} - 1)\{(N_I - l)f[S_I(k, l)]p_{k,l}(t)\}. \end{aligned} \quad (\text{A4})$$

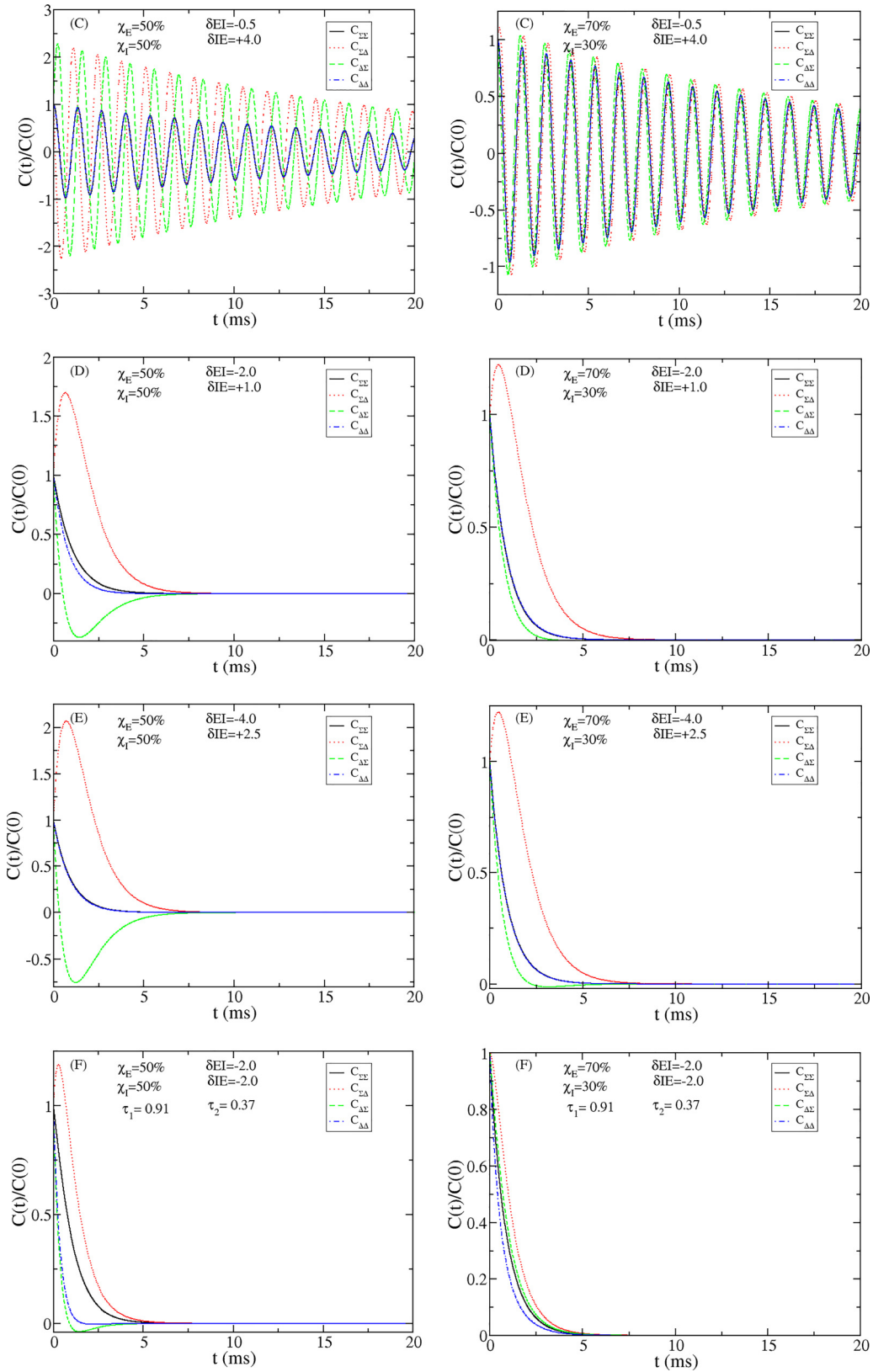


FIG. 6. The auto- and cross-correlation functions at the different points in the parameter space (Fig. 2). The left column data are for systems with $\chi_E = \chi_I = 50\%$, whereas the right column is for $\chi_E = 70\%$ and $\chi_I = 30\%$. Parameters are $w_{EE} = 6.95$, $w_{II} = 6.85$, $h = 10^{-6}$, $\alpha = 0.1$, $w_{EI} = w_{II} + \delta EI$, and $w_{IE} = w_{EE} + \delta IE$.

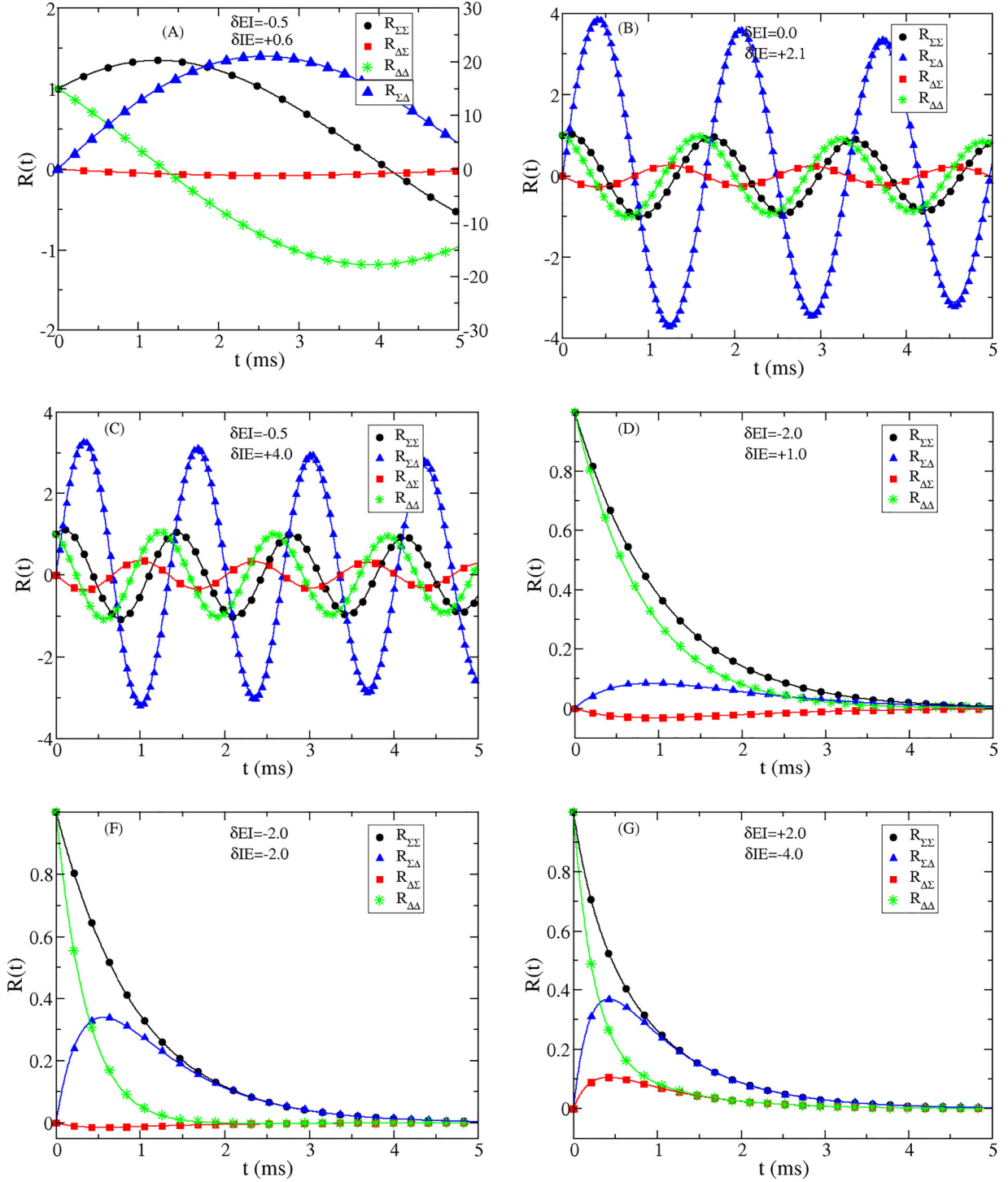


FIG. 7. The response functions for $\chi_E = \chi_I = 50\%$ evaluated at different points A, B, C, D, F, and G in the phase diagram (Fig. 2). The symbols are for numerical data ($N = 10^{14}$), with parameters $w_{EE} = 6.95$, $w_{II} = 6.85$, $h = 10^{-6}$, $\alpha = 0.1$, $w_{EI} = w_{II} + \delta EI$, and $w_{IE} = w_{EE} + \delta IE$, whereas solid lines represent analytical results. The range of values for $R_{\Sigma\Delta}$ is $[-30:30]$ only for point A. Details of simulations are reported in Sec. II B.

Finally we have

$$\begin{aligned} \frac{dp_{k,l}(t)}{dt} = & -\partial_k \left[N \chi_E A_E \left(\frac{k}{N_E}, \frac{l}{N_I} \right) p_{k,l}(t) \right] + \frac{1}{2} \partial_k^2 \left[N \chi_E D_E \left(\frac{k}{N_E}, \frac{l}{N_I} \right) p_{k,l}(t) \right] - \frac{1}{3!} \partial_k^3 \left[N \chi_E A_E \left(\frac{k}{N_E}, \frac{l}{N_I} \right) p_{k,l}(t) \right] + \dots \\ & - \partial_l \left[N \chi_I A_I \left(\frac{k}{N_E}, \frac{l}{N_I} \right) p_{k,l}(t) \right] + \frac{1}{2} \partial_l^2 \left[N \chi_I D_I \left(\frac{k}{N_E}, \frac{l}{N_I} \right) p_{k,l}(t) \right] - \frac{1}{3!} \partial_l^3 \left[N \chi_I A_I \left(\frac{k}{N_E}, \frac{l}{N_I} \right) p_{k,l}(t) \right] + \dots, \quad (\text{A5}) \end{aligned}$$

where

$$A_E(x, y) = -\alpha x + (1-x)f(w_{EE}x - w_{EI}y + h_E), \quad (\text{A6})$$

$$D_E(x, y) = \alpha x + (1-x)f(w_{EE}x - w_{EI}y + h_E), \quad (\text{A7})$$

$$A_I(x, y) = -\alpha y + (1-y)f(w_{IE}x - w_{II}y + h_I), \quad (\text{A8})$$

$$D_I(x, y) = \alpha y + (1-y)f(w_{IE}x - w_{II}y + h_I), \quad (\text{A9})$$

with $x = \frac{k}{N_E}$, $y = \frac{l}{N_I}$, $\chi_E = \frac{N_E}{N}$, and $\chi_I = \frac{N_I}{N}$.

Now for $p_{k,l}(t) = \pi(\xi_E, \xi_I, t)$, we can write

$$\begin{aligned} \frac{\partial p_{k,l}(t)}{\partial t} &= \frac{\partial}{\partial t} \pi(\xi_E, \xi_I, t) + \frac{\partial}{\partial t} \xi_E \frac{\partial}{\partial \xi_E} \pi(\xi_E, \xi_I, t) \\ &\quad + \frac{\partial}{\partial t} \xi_I \frac{\partial}{\partial \xi_I} \pi(\xi_E, \xi_I, t). \end{aligned} \quad (\text{A10})$$

Considering that $\partial_t \xi_E = -N_E^{1/2} \partial_t E$ and $\partial_t \xi_I = -N_I^{1/2} \partial_t I$, from Eq. (A10) we can write

$$\begin{aligned} \partial_t p_{k,l}(t) &= \partial_t \pi(\xi_E, \xi_I, t) - N_E^{1/2} \partial_t E \partial_{\xi_E} \pi(\xi_E, \xi_I, t) \\ &\quad - N_I^{1/2} \partial_t I \partial_{\xi_I} \pi(\xi_E, \xi_I, t). \end{aligned} \quad (\text{A11})$$

Next, by Taylor's expanding $A_{E,I}$ and $D_{E,I}$ in powers of the system size, the leading term of the order $N^{1/2}$ provides the deterministic equations

$$\begin{aligned} -N^{1/2} \chi_E^{1/2} \partial_t E \partial_{\xi_E} \pi &= -N^{1/2} \chi_E^{1/2} A_E(E, I) \partial_{\xi_E} \pi \\ -N^{1/2} \chi_I^{1/2} \partial_t I \partial_{\xi_I} \pi &= -N^{1/2} \chi_I^{1/2} A_I(E, I) \partial_{\xi_I} \pi, \end{aligned} \quad (\text{A12})$$

$$\begin{aligned} \frac{dE}{dt} &= -\alpha E + (1-E)f(S_E), \\ \frac{dI}{dt} &= -\alpha I + (1-I)f(S_I), \end{aligned} \quad (\text{A13})$$

whereas the successive term of the order N^0 provides the Fokker-Planck equations

$$\begin{aligned} \partial_t \pi &= -[A_{E,E}(E, I) \partial_{\xi_E} (\xi_E \pi) + \sqrt{\chi_E/\chi_I} A_{E,I}(E, I) \\ &\quad \times \partial_{\xi_E} (\xi_I \pi) + \sqrt{\chi_I/\chi_E} A_{I,E}(E, I) \partial_{\xi_I} (\xi_I \pi) + A_{I,I}(E, I) \\ &\quad \times \partial_{\xi_I} (\xi_I \pi)] + \frac{1}{2} D_E(E, I) \partial_{\xi_E}^2 \pi + \frac{1}{2} D_I(E, I) \partial_{\xi_I}^2 \pi. \end{aligned} \quad (\text{A14})$$

This approximation, which drops all successive terms, is called "linear noise approximation" and can be rewritten as two coupled Langevin equations

$$\frac{d}{dt} \begin{pmatrix} \xi_E \\ \xi_I \end{pmatrix} = \tilde{\mathbf{A}} \begin{pmatrix} \xi_E \\ \xi_I \end{pmatrix} + \tilde{\mathbf{D}} \begin{pmatrix} \eta_E \\ \eta_I \end{pmatrix}, \quad (\text{A15})$$

where $\tilde{\mathbf{A}} = \begin{pmatrix} A_{E,E}(E, I) & \sqrt{\chi_E/\chi_I} A_{E,I}(E, I) \\ \sqrt{\chi_I/\chi_E} A_{I,E}(E, I) & A_{I,I}(E, I) \end{pmatrix}$ with

$$A_{E,E}(E, I) = -\alpha - f(S_E) + (1-E)w_{EE}f'(S_E), \quad (\text{A16})$$

$$A_{E,I}(E, I) = -(1-E)w_{EI}f'(S_E), \quad (\text{A17})$$

$$A_{I,E}(E, I) = (1-I)w_{IE}f'(S_I), \quad (\text{A18})$$

$$A_{I,I}(E, I) = -\alpha - f(S_I) - (1-I)w_{II}f'(S_I), \quad (\text{A19})$$

$$D_E(E, I) = \sqrt{\alpha E + (1-E)f(S_E)}, \quad (\text{A20})$$

$$D_I(E, I) = \sqrt{\alpha I + (1-I)f(S_I)}, \quad (\text{A21})$$

and, $\tilde{\mathbf{D}} = \begin{pmatrix} D_E & 0 \\ 0 & D_I \end{pmatrix}$, where at the fixed point, $D_E = \sqrt{2\alpha E_0}$ and $D_I = \sqrt{2\alpha I_0}$.

By introducing the variable change from (E, I) to (Σ, Δ) , it is possible to obtain the set of deterministic equations (5), and from Eq. (A15) the two coupled Langevin equations for the fluctuating terms

$$\frac{d}{dt} \begin{pmatrix} \xi_\Sigma \\ \xi_\Delta \end{pmatrix} = \mathbf{A} \begin{pmatrix} \xi_\Sigma \\ \xi_\Delta \end{pmatrix} + \mathbf{D} \begin{pmatrix} \eta_\Sigma \\ \eta_\Delta \end{pmatrix}, \quad (\text{A22})$$

where

$$\begin{pmatrix} \xi_\Sigma \\ \xi_\Delta \end{pmatrix} = \begin{pmatrix} \chi_E & \chi_I \\ \chi_E & -\chi_I \end{pmatrix} \begin{pmatrix} \xi_E \\ \xi_I \end{pmatrix}, \quad (\text{A23})$$

$$\begin{aligned} \mathbf{A} &= \begin{pmatrix} \chi_E & \chi_I \\ \chi_E & -\chi_I \end{pmatrix} \begin{pmatrix} A_{E,E}(E, I) & \sqrt{\chi_E/\chi_I} A_{E,I}(E, I) \\ \sqrt{\chi_I/\chi_E} A_{I,E}(E, I) & A_{I,I}(E, I) \end{pmatrix} \\ &\quad \times \frac{1}{2} \begin{pmatrix} \frac{1}{\chi_E} & \frac{1}{\chi_E} \\ \frac{1}{\chi_I} & -\frac{1}{\chi_I} \end{pmatrix} = \begin{pmatrix} x & y \\ z & w \end{pmatrix} \end{aligned} \quad (\text{A24})$$

with $x = \frac{1}{2}[A_{E,E}(E, I) + (\frac{\chi_E}{\chi_I})^{3/2}A_{E,I}(E, I) + (\frac{\chi_I}{\chi_E})^{3/2}A_{I,E}(E, I) + A_{I,I}(E, I)]$, $y = \frac{1}{2}[A_{E,E}(E, I) - (\frac{\chi_E}{\chi_I})^{3/2}A_{E,I}(E, I) + (\frac{\chi_I}{\chi_E})^{3/2}A_{I,E}(E, I) - A_{I,I}(E, I)]$, $z = \frac{1}{2}[A_{E,E}(E, I) + (\frac{\chi_E}{\chi_I})^{3/2}A_{E,I}(E, I) - (\frac{\chi_I}{\chi_E})^{3/2}A_{I,E}(E, I) - A_{I,I}(E, I)]$, and $w = \frac{1}{2}[A_{E,E}(E, I) - (\frac{\chi_E}{\chi_I})^{3/2}A_{E,I}(E, I) - (\frac{\chi_I}{\chi_E})^{3/2}A_{I,E}(E, I) + A_{I,I}(E, I)]$. Moreover,

$$\begin{aligned} \mathbf{D} &= \begin{pmatrix} \chi_E & \chi_I \\ \chi_E & -\chi_I \end{pmatrix} \begin{pmatrix} D_E & 0 \\ 0 & D_I \end{pmatrix} \frac{1}{2} \begin{pmatrix} \frac{1}{\chi_E} & \frac{1}{\chi_E} \\ \frac{1}{\chi_I} & -\frac{1}{\chi_I} \end{pmatrix} \\ &= \frac{1}{2} \begin{pmatrix} D_E + D_I & D_E - D_I \\ D_E - D_I & D_E + D_I \end{pmatrix}. \end{aligned} \quad (\text{A25})$$

The noise amplitude matrix can be written as

$$\mathcal{M} = \mathbf{D}\mathbf{D}^T = \begin{pmatrix} G & H \\ H & G \end{pmatrix}, \quad (\text{A26})$$

where at the fixed points $G = \frac{1}{2}(D_E^2 + D_I^2) = \alpha E_0 + \alpha I_0$ and $H = \frac{1}{2}(D_E^2 - D_I^2) = \alpha E_0 - \alpha I_0$. Equation (A22) can be written in more compact form as

$$\frac{d\mathbf{X}}{dt} = \mathbf{A}\mathbf{X} + \mathbf{D}\boldsymbol{\eta}, \quad (\text{A27})$$

where $\mathbf{X} \equiv (\xi_\Sigma, \xi_\Delta)$ and $\boldsymbol{\eta} \equiv (\eta_\Sigma, \eta_\Delta)$. Then we can write the solutions of the above equation as

$$\mathbf{X}(t) = e^{\mathbf{A}t} \mathbf{X}(0) + \mathbf{D} \int_0^t dt' e^{\mathbf{A}(t-t')} \boldsymbol{\eta}(t'), \quad (\text{A28})$$

valid for $t \geq 0$.

2. Correlation functions

The correlation matrix for the fluctuating terms is defined as

$$C_{ij}(t) \equiv \langle \xi_i(t) \xi_j(0) \rangle = (e^{\mathbf{A}t} \boldsymbol{\sigma})_{ij}, \quad (\text{A29})$$

where $\sigma_{ij} = \langle \xi_i(0)\xi_j(0) \rangle$ are the components of the covariance matrix which satisfies

$$\mathcal{M} = \frac{\mathbf{A}\sigma + \sigma\mathbf{A}^T}{2}. \tag{A30}$$

The covariance matrix can be written as

$$\sigma = \begin{pmatrix} \sigma_{11} & \sigma_{12} \\ \sigma_{21} & \sigma_{22} \end{pmatrix}, \tag{A31}$$

where

$$\sigma_{11} = \frac{G - \sigma_{12}y}{x}, \tag{A32}$$

$$\sigma_{12} = \sigma_{21} = -\frac{G(zw + xy) - 2Hxw}{(x + w)(xw - yz)}, \tag{A33}$$

$$\sigma_{22} = \frac{G - \sigma_{12}z}{w}. \tag{A34}$$

The eigenvalues of the matrix \mathbf{A} are $\lambda_{\pm} = \frac{1}{2}[(x + w) \pm \sqrt{-\Theta}]$, where $\sqrt{-\Theta} = \sqrt{(x - w)^2 + 4yz}$.

To evaluate $e^{\mathbf{A}t}$ we need a diagonalizing matrix \mathbf{P} , which can be written as

$$\mathbf{P} = \begin{pmatrix} \frac{(x-\lambda_1)}{z\sqrt{1+[(x-\lambda_1)/z]^2}} & \frac{(x-\lambda_2)}{z\sqrt{1+[(x-\lambda_2)/z]^2}} \\ \frac{1}{\sqrt{1+[(x-\lambda_1)/z]^2}} & \frac{1}{\sqrt{1+[(x-\lambda_2)/z]^2}} \end{pmatrix}.$$

Now let $\mu = \sqrt{1 + [(x - \lambda_1)/z]^2}$ and $\nu = \sqrt{1 + [(x - \lambda_2)/z]^2}$, and then \mathbf{P} becomes

$$\mathbf{P} = \begin{pmatrix} \frac{x-\lambda_1}{z\mu} & \frac{x-\lambda_2}{z\nu} \\ \frac{1}{\mu} & \frac{1}{\nu} \end{pmatrix},$$

whose determinant is $|\mathbf{P}| = -\frac{\sqrt{-\Theta}}{z\mu\nu}$.

The inverse matrix of \mathbf{P} is

$$\begin{aligned} \mathbf{P}^{-1} &= -\frac{z\mu\nu}{\sqrt{-\Theta}} \begin{pmatrix} \frac{1}{\nu} & -\frac{x-\lambda_2}{z\nu} \\ -\frac{1}{\mu} & \frac{x-\lambda_1}{z\mu} \end{pmatrix} \\ &= \frac{1}{\sqrt{-\Theta}} \begin{pmatrix} -z\mu & (x - \lambda_2)\mu \\ z\nu & -(x - \lambda_1)\nu \end{pmatrix}. \end{aligned} \tag{A35}$$

Then we can write the matrix exponential as

$$\begin{aligned} e^{\mathbf{A}t} &= \mathbf{P}e^{\lambda_{\pm}t}\mathbf{P}^{-1} \\ &= \frac{1}{\sqrt{-\Theta}} \begin{pmatrix} \frac{x-\lambda_1}{z\mu} & \frac{x-\lambda_2}{z\nu} \\ \frac{1}{\mu} & \frac{1}{\nu} \end{pmatrix} \begin{pmatrix} e^{\lambda_2t} & 0 \\ 0 & e^{\lambda_1t} \end{pmatrix} \begin{pmatrix} -z\mu & (x - \lambda_2)\mu \\ z\nu & -(x - \lambda_1)\nu \end{pmatrix} \\ &= \frac{1}{\sqrt{-\Theta}} \begin{pmatrix} [(x - \lambda_2)e^{\lambda_1t} - (x - \lambda_1)e^{\lambda_2t}] & [y(e^{\lambda_1t} - e^{\lambda_2t})] \\ [z(e^{\lambda_1t} - e^{\lambda_2t})] & [(x - \lambda_2)e^{\lambda_2t} - (x - \lambda_1)e^{\lambda_1t}] \end{pmatrix}. \end{aligned} \tag{A36}$$

Now from Eq. (A29), calculating the matrix product, we obtain the four correlation functions reported in the main text.

3. Response functions

The response of the system is defined as $R_{ij}(t) \equiv \frac{\overline{\delta\xi_i(t)}}{\delta\xi_j(0)}$, with $(i, j) = (\Sigma, \Delta)$ as the response in ξ_i once an instantaneous perturbation in ξ_j is applied at $t = 0$. According to Eq. (A28), the response matrix is

$$\mathbf{R}(t) = e^{\mathbf{A}t}. \tag{A37}$$

From Eq. (A37), we see that the matrix exponential $e^{\mathbf{A}t}$ and the response function $\mathbf{R}(t)$ coincide; therefore from Eq. (A36) we can write the equations for the response functions as

$$R_{\Sigma\Sigma}(t) = \frac{1}{\sqrt{-\Theta}} [(x - \lambda_2)e^{\lambda_1t} - (x - \lambda_1)e^{\lambda_2t}],$$

$$R_{\Sigma\Delta}(t) = \frac{1}{\sqrt{-\Theta}} [y(e^{\lambda_1t} - e^{\lambda_2t})],$$

$$R_{\Delta\Sigma}(t) = \frac{1}{\sqrt{-\Theta}} [z(e^{\lambda_1t} - e^{\lambda_2t})],$$

$$R_{\Delta\Delta}(t) = \frac{1}{\sqrt{-\Theta}} [(x - \lambda_2)e^{\lambda_2t} - (x - \lambda_1)e^{\lambda_1t}]. \tag{A38}$$

In the case of complex eigenvalues $\lambda_{\pm} = a \pm ib$, where $a = (x + w)/2$ and $ib = \sqrt{-\Theta}/2$, we can write the response functions as

$$R_{\Sigma\Sigma}(t) = e^{at} \cos(bt) + \frac{(x - a)}{b} e^{at} \sin(bt),$$

$$R_{\Sigma\Delta}(t) = \frac{y}{b} e^{at} \sin(bt),$$

$$R_{\Delta\Sigma}(t) = \frac{z}{b} e^{at} \sin(bt),$$

$$R_{\Delta\Delta}(t) = e^{at} \cos(bt) - \frac{(x - a)}{b} e^{at} \sin(bt). \tag{A39}$$

[1] T Petermann, T. C. Thiagarajan, M. A. Lebedev, M. A. L. Nicolelis, D. R. Chialvo, and D. Pleniz, *Proc. Natl. Acad. Sci. USA* **106**, 15921 (2009).

[2] A. Mazzoni, F. D. Broccard, E. Garcia-Perez, P. Bonifazi, M. E. Ruaro, and V. Torre, *PLoS ONE* **2**, e439 (2007).

[3] G. Deco and V. K. Jirsa, *J. Neurosci.* **32**, 3366 (2012).

- [4] G. Deco, V. K. Jirsa, and A. R. McIntosh, *Nat. Rev. Neurosci.* **12**, 43 (2011).
- [5] A. Arieli, A. Sterkin, A. Grinvald, and A. Aertsen, *Science* **273**, 1868 (1996).
- [6] D. Papo, *Front. Syst. Neurosci.* **8**, 112 (2014).
- [7] A. Sarracino, O. Arviv, O. Shriki, and L. de Arcangelis, *Phys. Rev. Res.* **2**, 033355 (2020).
- [8] U. M. B. Marconi, A. Puglisi, L. Rondoni, and A. Vulpiani, *Phys. Rep.* **461**, 111 (2008).
- [9] A. Puglisi, A. Sarracino, and A. Vulpiani, *Phys. Rep.* **709–710**, 1 (2017).
- [10] K. Sato, Y. Ito, T. Yomo, and K. Kaneko, *Proc. Natl. Acad. Sci. USA* **100**, 14086 (2003).
- [11] M. Chen, L. R. Niestemski, R. Prevost, M. McRae, S. Cholleti, G. Najarro, T. G. Buchman, and M. W. Deem, *Phys. Biol.* **10**, 016006 (2013).
- [12] B. Lindner, *Phys. Rev. Lett.* **129**, 198101 (2022).
- [13] H. R. Wilson and J. D. Cowan, *Biophys. J.* **12**, 1 (1972).
- [14] J. D. Cowan, J. Neuman, and W. van Drongelen, *J. Math. Neurosci.* **6**, 1 (2016).
- [15] M. Benayoun, J. Cowan, D. W. van, and E. Wallace, *PLoS Comput. Biol.* **6**, e1000846 (2010).
- [16] A. de Candia, A. Sarracino, I. Apicella, and L. de Arcangelis, *PLoS Comput. Biol.* **17**, e1008884 (2021).
- [17] I. Apicella, S. Scarpetta, L. de Arcangelis, A. Sarracino, and A. de Candia, *Sci. Rep.* **12**, 21870 (2022).
- [18] D. Raimo, A. Sarracino, and L. de Arcangelis, *Physica A* **565**, 125555 (2021).
- [19] M. K. Nandi, A. Sarracino, H. J. Herrmann, and L. de Arcangelis, *Phys. Rev. E* **106**, 024304 (2022).
- [20] E. Wallace, M. Benayoun, W. van Drongelen, and J. D. Cowan, *PLoS ONE* **6**, e14804 (2011).
- [21] P. C. Bressloff, *Phys. Rev. E* **82**, 051903 (2010).
- [22] I. I. Lima Dias Pinto and M. Copelli, *Phys. Rev. E* **100**, 062416 (2019).
- [23] C. Zankoc, T. Biancalani, D. Fanelli, and R. Livi, *Chaos, Solitons Fractals* **103**, 504 (2017).
- [24] H. C. Piuvezam, B. Marin, M. Copelli, and M. A. Muñoz, [arXiv:2301.06839](https://arxiv.org/abs/2301.06839).
- [25] J.-y. Wu, L. Guan, and Y. Tsau, *J. Neurosci.* **19**, 5005 (1999).
- [26] D. Plenz and S. Kitai, *J. Neurophysiol.* **76**, 4180 (1996).
- [27] K. Linkenkaer-Hansen, V. V. Nikouline, J. M. Palva, and R. J. Ilmoniemi, *J. Neurosci.* **21**, 1370 (2001).
- [28] J. D. Murray, A. Bernacchia, D. J. Freedman, R. Romo, J. D. Wallis, X. Cai, C. Padoa-Schioppa, T. Pasternak, H. Seo, D. Lee, and X.-J. Wang, *Nat. Neurosci.* **17**, 1661 (2014).
- [29] P. C. Bressloff, *SIAM J. Appl. Math.* **70**, 1488 (2010).
- [30] T. Ohira and J. Cowan, in *Mathematics of Neural Networks: Models, Algorithms, and Applications*, edited by S. Ellacort and I. Anderson (Springer, Berlin, 1997), p. 290.
- [31] A. Crisanti, A. Puglisi, and D. Villamaina, *Phys. Rev. E* **85**, 061127 (2012).
- [32] A. Sarracino, D. Villamaina, G. Gradenigo, and A. Puglisi, *Europhys. Lett.* **92**, 34001 (2010).
- [33] D. T. Gillespie, *J. Phys. Chem.* **81**, 2340 (1977).
- [34] S. Zhou and Y. Yu, *Front. Neurosci.* **12**, 46 (2018).
- [35] J. S. Isaacson and M. Scanziani, *Neuron* **72**, 231 (2011).
- [36] A. Bhatia, S. Moza, and U. Bhalla, *eLife* **8**, e43415 (2019).
- [37] H.-y. He and H. T. Cline, *J. Exp. Neurosci.* **13**, 1 (2019).
- [38] J. M. Beggs and D. Plenz, *J. Neurosci.* **23**, 11167 (2003).
- [39] P. Massobrio, L. de Arcangelis, V. Pasquale, H. Jensen, and D. Plenz, *Front. Syst. Neurosci.* **9**, 22 (2015).
- [40] F. Lombardi, H. J. Herrmann, C. Perrone-Capano, D. Plenz, and L. de Arcangelis, *Phys. Rev. Lett.* **108**, 228703 (2012).
- [41] F. Lombardi, H. J. Herrmann, and L. de Arcangelis, *Chaos* **27**, 047402 (2017).